

Neutron skin of neutron-rich nuclei

I. A. M. Abdul-Magead  and Badawy Abu-Ibrahim *

Department of Physics, Cairo University, Giza 12613, Egypt



(Received 15 November 2021; revised 20 December 2021; accepted 14 January 2022; published 26 January 2022)

An extension to our previous method to deduce the neutron radii of neutron-rich nuclei is presented. This method requires measuring the reaction cross sections of both the neutron-rich nucleus and its stable isotope at the same energy per nucleon on a carbon target. Using this method and the available experimental data, the neutron radii of $^{21-29}\text{F}$, $^{21-32}\text{Ne}$, $^{24-35}\text{Na}$, $^{25-38}\text{Mg}$, and $^{45-51}\text{Ca}$ isotopes have been deduced. The neutron skin of these isotopes (in the mass region $A = 21-51$) exhibited a linear relationship with the isospin $(N - Z)/A$ at a slope equal to 3.216 ± 0.11 fm. This tends to be much larger than that previously reported for nuclei in the mass region $A = 40-238$ at 0.9 ± 0.15 fm.

DOI: [10.1103/PhysRevC.105.014626](https://doi.org/10.1103/PhysRevC.105.014626)

I. INTRODUCTION

Determination of neutron radii is highly important in both nuclear physics and astrophysics. Neutron radii are essential to extract the neutron skin thickness. The neutron skin thickness of nuclei is a sensitive probe of the nuclear symmetry energy and has multiple implications for nuclear and astrophysical studies [1,2]. However, precision measurements of neutron radii are difficult to obtain. Recently, we proposed a new method to deduce the neutron radii of neutron-rich nuclei [3]. This method requires measuring the reaction cross sections of both the neutron-rich nucleus and its stable isotope at the same energy per nucleon on a proton target. Using this method we successfully determined the neutron radii of both ^{22}C and ^{14}Be .

Experimentalists prefer a carbon target to study neutron-rich isotopes due to technical difficulties. Most of the available experimental reaction/interaction cross section data are measured with a carbon target. This encouraged us to extend our method to involve a carbon target.

In this paper, we extend our previous work [3] so that one can use the reaction cross section (or interaction cross section) of the given isotope with a carbon target to obtain the neutron radii of the given isotope. Meanwhile, we assume the carbon target to be a point particle and introduce a profile function Γ_{NT} for the nucleon-target (NT) scattering [4].

In this approach, to obtain the neutron radius of a neutron-rich nucleus, one needs only the difference between the reaction cross sections of the studied neutron-rich nucleus and its stable isotope on a carbon target at the same energy per nucleon. We demonstrated the efficiency of the method by applying it to determine the neutron radii of fluorine, neon, sodium, magnesium, and calcium isotopes.

II. THE THEORETICAL FRAMEWORK

The total reaction cross section of a nucleus ($A = p + n$) incident on a carbon target is expressed in the optical limit

approximation (OLA) of Glauber theory [5] as b

$$\sigma_A^{\text{R}} = \int d\vec{b} (1 - e^{-2\text{Im}[\chi_A(\vec{b})]}), \quad (1)$$

where \vec{b} is the impact parameter vector perpendicular to the beam (z) direction, and $\chi(\vec{b})$ is the phase-shift function.

The OLA does not properly account for the breakup effect, which is important for loosely coupled nuclei. It overestimates the cross section, which tends to predict smaller radii for loosely bound nuclei [6]. To overcome this problem, several improvements to the OLA have been introduced [4,6,7]. In this regard, nucleon-target (NT) scattering is considered as an elementary vehicle in the Glauber theory [4]. Assuming the target as a scatterer, the authors have introduced a profile function Γ_{NT} for the NT scattering [4]. In this formalism, various effects such as the Fermi motion, Pauli correlations, short range dynamic correlations, etc., would be automatically included to some extent in the NT amplitude. Accordingly, the phase-shift function is defined as $i\chi_A(\vec{b}) = -\int d\vec{s} \rho_A(\vec{s}) \Gamma_{\text{NT}}(\vec{s} + \vec{b})$, where, ρ_A is the projectile density. In addition, the profile function Γ_{NT} for the nucleon- ^{12}C interaction appears in the form given by

$$\Gamma_{\text{NT}}(\vec{b}) = \sum_{j=1}^m \frac{1 - i\alpha_j}{4\pi\beta_j} \sigma_j^{\text{tot}} e^{-b^2/(2\beta_j)}, \quad (2)$$

where the parameters σ_j , β_j , and α_j are determined by fitting the experimental elastic angular distribution as well as the total and reaction cross sections of protons incident on a carbon target.

Besides, the reaction cross section shift between a neutron-rich nucleus (A_2) and its stable isotope (A_1) is defined as $\delta\sigma_{A_2,A_1}^{\text{R}} = \sigma_{A_2}^{\text{R}} - \sigma_{A_1}^{\text{R}}$. Both $\sigma_{A_2}^{\text{R}}$ and $\sigma_{A_1}^{\text{R}}$ are measured on a carbon target and at the same energy per nucleon. From Eq. (1), the reaction cross section shift is given by

$$\delta\sigma_{A_2,A_1}^{\text{R}} = 2\pi \int_0^\infty b e^{-2\text{Im}[\chi_{A_1}(\vec{b})]} (1 - e^{-2\text{Im}[\chi_{A_2}(\vec{b})]}) db, \quad (3)$$

* aibrahim@sci.cu.edu.eg

TABLE I. Parameters of proton- ^{12}C profile functions used in the present calculations; see Eq. (2). The total and reaction cross sections, σ_T and σ_R , calculated by the profile functions are also shown. The experimental values are shown in parentheses [18].

| T_p (MeV) | σ_T (mb) | σ_R (mb) | σ (fm 2) | β (fm 2) | α |
|-------------|-----------------|--------------------|---------------------|--------------------|-------------------|
| 250 | 285 | 202 (202 \pm 20) | 39.354 -9.8799 | 2.0182 0.95994 | -0.016 -0.4033 |
| 300 | 284 | 189 | 39.986 -11.562 | 1.8393 1.0348 | 0.5856 0.91887 |

where $\Delta\chi_A(\vec{b}) = \chi_{A_2}(\vec{b}) - \chi_{A_1}(\vec{b})$ and

$$-2 \operatorname{Im}[\Delta\chi_A(\vec{b})] = -\sum_{j=1}^m \frac{\sigma_j^{\text{tot}}}{2\pi\beta_j} \int d\vec{s} [\rho_{A_2}(\vec{s}) - \rho_{A_1}(\vec{s})] e^{-i(\vec{b}+\vec{s})^2/(2\beta_j)}. \quad (4)$$

In accordance with recent experimental data for the proton radii of calcium isotopes [3], the point proton density distribution for both A_2 and A_1 are taken to be nearly the same. The maximum difference between proton radii of Ca isotopes ($A = 40$ – 52) is reported to be ultimately 0.077 fm [8] while that for Al isotopes ($A = 27$ – 32) attains 0.05 fm [9]. This means that $\rho_{A_2} - \rho_{A_1} \simeq \rho_{n_2} - \rho_{n_1}$, with ρ_{n_2} and ρ_{n_1} representing the neutron densities of A_2 and A_1 , respectively. Thereupon, Eq. (3) reduces to

$$\delta\sigma_{A_2,A_1}^R \simeq 2\pi \int_0^\infty b e^{-2\operatorname{Im}[\chi_{A_1}(b)]} (1 - e^{-2\operatorname{Im}[\Delta\chi_n(b)]}) db. \quad (5)$$

It is worth noting that the proton density of the neutron-rich isotope has no bearing on the ensuing phase shift. In Eq. (5), the neutron and proton density distributions of the stable isotope can be obtained from literature [10,11], while still the neutron density distribution of the neutron-rich isotope is the key quantity.

TABLE II. Reaction cross section (in mb) of nucleus- ^{12}C at $E = 250$ MeV/ n for the projectile stable nuclei ^{19}F , ^{20}Ne , ^{23}Na , ^{24}Mg , and at $E = 300$ MeV/ n for ^{42}Ca .

| Nucleus | Expt. data | Our work |
|------------------|--------------------|----------|
| ^{19}F | 1031 \pm 15 [19] | 1066 |
| ^{20}Ne | 1053 \pm 10 [20] | 1091 |
| ^{23}Na | 1122 \pm 11 [21] | 1155 |
| ^{24}Mg | 1173 \pm 27 [22] | 1177 |
| ^{42}Ca | 1463 [16] | 1459 |

To check the validity of the approximation in Eq. (5), we define the FS factor as

$$\text{FS} = \frac{\delta\sigma_{A_2,A_1}^R[\text{Eq. (3)}] - \delta\sigma_{A_2,A_1}^R[\text{Eq. (5)}]}{\delta\sigma_{A_2,A_1}^R[\text{Eq. (3)}]} \times 100\%, \quad (6)$$

which gives the percentage deviation of $\delta\sigma_{A_2,A_1}^R$ calculated using Eq. (5) from the exact values obtained from Eq. (3).

III. RESULTS

Except for calcium isotopes (280 MeV/ n), most of the experimental reaction (interaction) cross section data used in this paper are measured around 250 MeV/ n . Therefore, we first determine the parameters of first two Γ_{NT} terms by fitting p - ^{12}C elastic scattering reaction cross section and total cross section experimental data at 250 MeV as listed in Table I. Harmonic oscillator (HO) density distribution is considered for ^{12}C . The configuration of the ^{12}C wave function is assumed to be $(0s_{1/2})^2(0p_{3/2})^4$ for both protons and neutrons. The HO length parameter is fixed in such a way as to reproduce the proton (neutron) radius, 2.33 (2.30) fm [12], extracted from the charge radius. Figure 1(a) shows the differential cross section of p - ^{12}C at $T_p = 250$ MeV. The solid curve is the phenomenological fit by Eq. (2), whose parameters are listed in Table I. As we can see Γ_{NT} reproduces

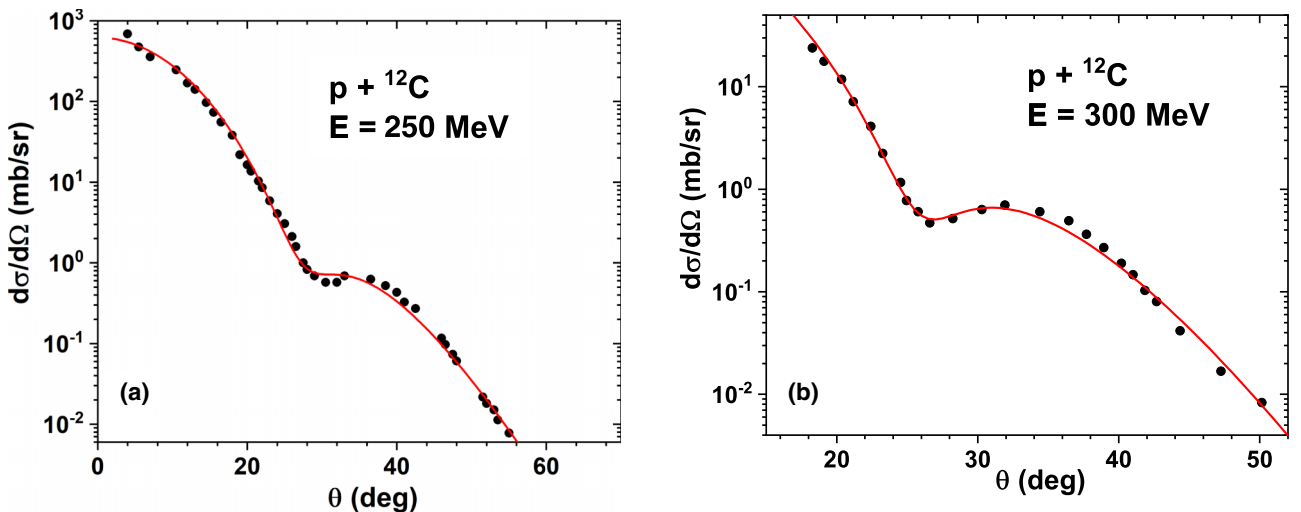


FIG. 1. The elastic differential cross section of p - ^{12}C at 250 MeV (a) and at 300 MeV (b). The solid curve is a phenomenological fit of Eq. (2). The data are taken from Ref. [23].

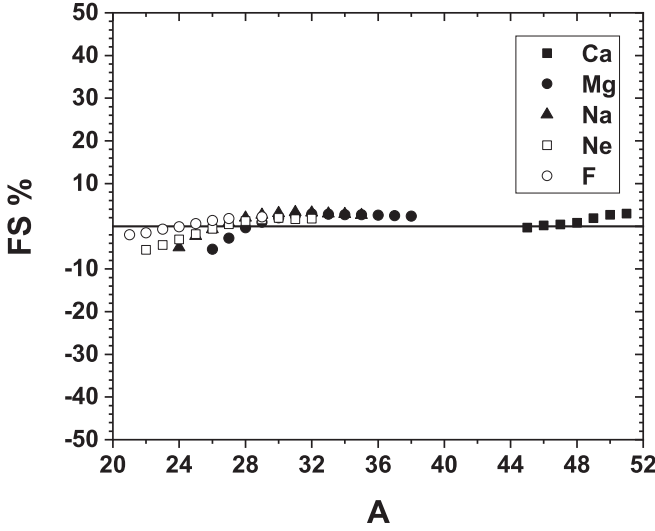


FIG. 2. The FS factor against the mass number A , calculated with Eq. (6) for F, Ne, Na, Mg, and Ca at 250 MeV/ n .

the experimental data fairly well. Also, using Eqs. (1) and (2) we calculated the reaction cross section of $^{12}\text{C}-^{12}\text{C}$ and obtained a value of 822 mb, which is in good agreement with the experimental values 873 ± 60 mb [13,14] and 786 mb [15]. For calcium isotopes, the available experimental data are at 280 MeV/ n [16] whereas the nearest experimental data we found for $p-^{12}\text{C}$ scattering are at 300 MeV/ n . The best fit of the experimental elastic angular distribution as well as the total and reaction cross sections of $p-^{12}\text{C}$ scattering by Eq. (2) yields the parameters listed in Table I. Correspondingly, Fig. 1(b) shows the differential cross section of $p-^{12}\text{C}$ at $T_p = 300$ MeV. The solid curve is the phenomenological fit by Eq. (2). The calculated reaction cross section of $^{12}\text{C}-^{12}\text{C}$ at 300 MeV/ n using Eqs. (1) and (2) is found to be 786 mb, while the experimental value is 858 ± 60 mb [13]. In addition, the reaction cross sections obtained according to Eqs. (1) and (2) for all the stable nuclei, ^{20}Ne , ^{23}Na , ^{24}Mg , and ^{42}Ca , with

densities from Hartree-Fock-Bogoliubov calculations with the BSK2 Skyrme force [17] on the ^{12}C target, are in good agreement with the corresponding experimental data, as shown in Table II.

To assess the validity of the approximation given in Eq. (5), we calculated the FS factor for all the nuclei studied in this paper at 250 MeV/ n . Figure 2 reveals a maximum percentage error about 5% with respect to the exact calculations using [Eq. (3)].

We apply the proposed method to determine the neutron radii of fluorine ($A = 21-29$), neon ($A = 21-32$), sodium ($A = 24-35$), magnesium ($A = 25-38$), and calcium ($A = 45-51$) isotopes. We used two types of point-neutron density distributions: harmonic oscillator (HO) and two-parameter Fermi (2pF) densities. Assuming the usual shell model structure for all the studied isotopes, a suitable neutron configuration for the ground state is adopted for the HO wave function. Then, the HO length parameter is varied to fit the experimental reaction cross section shift. On the other hand, in case of 2pF density distribution, we fixed the diffuseness parameter to be 0.49 fm [16]. Also, the density constant ρ_0 is determined from its normalization to neutron number, while the half-density radius is varied to fit the experimental reaction cross section shift.

For fluorine isotopes, the stable nucleus is ^{19}F , and the neutron and proton radii are taken to be 2.83 fm and 2.78 fm respectively, as calculated using Hartree-Fock-Bogoliubov with the BSK2 Skyrme force [17]. The reaction cross sections of ^{19}F and ^{29}F on a carbon target are measured and found to be 1031 ± 15 [19] and 1396 ± 28 mb [24], respectively. Thus, the reaction cross section shift for ^{29}F and ^{19}F incident on a carbon target at 240 MeV/ n is $\delta\sigma_{29,19}^R[\text{Expt.}] = 365 \pm 43$ mb. Meanwhile, a HO wave function is assumed for ^{29}F , with the neutron configuration for the ground state being $(0s_{1/2})^2(0p_{3/2})^4(0p_{1/2})^2(0d_{5/2})^6(0d_{3/2})^4(1s_{1/2})^2$.

Figure 3 shows the reaction cross section shift $\delta\sigma_{29,19}^R$ as a function of the neutron radius of ^{29}F using HO density

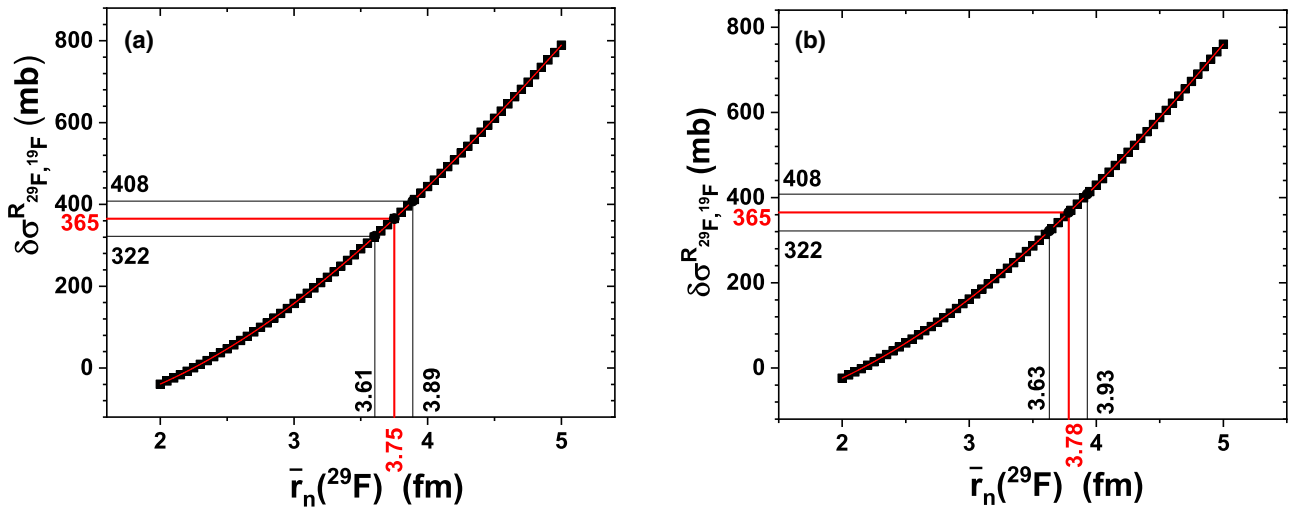


FIG. 3. The reaction cross section shift $\delta\sigma_{29,19}^R$ as a function of the neutron radius of ^{29}F , using HO density (a) and using 2pF density (b).

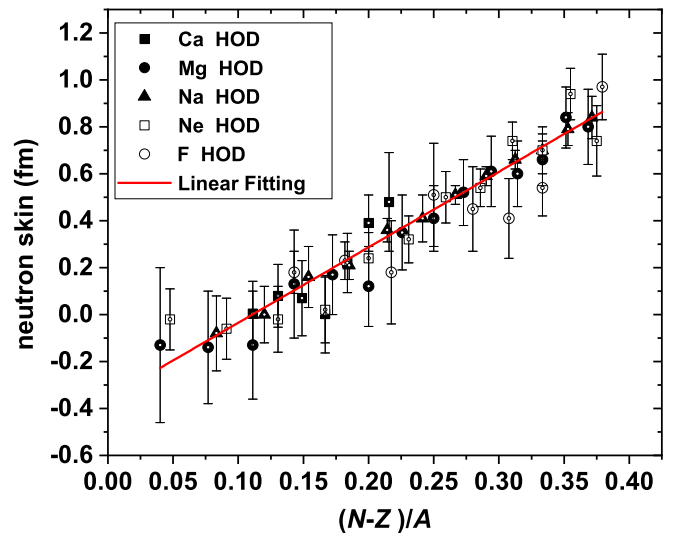
TABLE III. The root-mean-square neutron radii $\langle r_n^2 \rangle^{1/2}$ in units of fm for fluorine, neon, sodium, magnesium, and calcium isotopes; the first column represents the neutron number of each isotope.

| N | F | | Ne | | Na | | Mg | | Ca | |
|-----|-----------------|------|-----------------|------|-----------------|------|-----------------|------|-----------------|------|
| | Our work | BSK2 |
| 11 | | | 2.84 ± 0.13 | 2.88 | | | | | | |
| 12 | 2.96 ± 0.09 | 2.96 | 2.80 ± 0.13 | 2.94 | | | | | | |
| 13 | 3.01 ± 0.08 | 3.00 | 2.84 ± 0.14 | 2.99 | 2.83 ± 0.16 | 2.98 | 2.84 ± 0.33 | 2.98 | | |
| 14 | 2.96 ± 0.22 | 3.06 | 2.88 ± 0.14 | 3.04 | 2.91 ± 0.12 | 3.03 | 2.83 ± 0.24 | 3.03 | | |
| 15 | 3.29 ± 0.22 | 3.12 | 3.10 ± 0.11 | 3.10 | 3.07 ± 0.13 | 3.09 | 2.84 ± 0.23 | 3.08 | | |
| 16 | 3.23 ± 0.18 | 3.21 | 3.18 ± 0.10 | 3.18 | 3.12 ± 0.06 | 3.16 | 3.10 ± 0.23 | 3.14 | | |
| 17 | 3.19 ± 0.17 | 3.28 | 3.36 ± 0.11 | 3.24 | 3.27 ± 0.05 | 3.22 | 3.14 ± 0.17 | 3.20 | | |
| 18 | 3.32 ± 0.12 | 3.35 | 3.40 ± 0.08 | 3.31 | 3.32 ± 0.10 | 3.28 | 3.09 ± 0.17 | 3.26 | | |
| 19 | | | 3.60 ± 0.08 | 3.37 | 3.42 ± 0.04 | 3.34 | 3.32 ± 0.16 | 3.31 | | |
| 20 | 3.75 ± 0.14 | 3.48 | 3.56 ± 0.10 | 3.43 | 3.50 ± 0.04 | 3.39 | 3.38 ± 0.14 | 3.36 | | |
| 21 | | | 3.80 ± 0.11 | 3.58 | 3.57 ± 0.04 | 3.43 | 3.49 ± 0.14 | 3.41 | | |
| 22 | | | 3.60 ± 0.15 | 3.57 | 3.61 ± 0.04 | 3.49 | 3.58 ± 0.15 | 3.46 | | |
| 23 | | | | | 3.70 ± 0.07 | 3.54 | 3.57 ± 0.14 | 3.50 | | |
| 24 | | | | | 3.75 ± 0.09 | 3.61 | 3.63 ± 0.11 | 3.55 | | |
| 25 | | | | | | | 3.81 ± 0.13 | 3.60 | 3.43 ± 0.14 | 3.53 |
| 26 | | | | | | | 3.77 ± 0.16 | 3.65 | 3.51 ± 0.13 | 3.56 |
| 27 | | | | | | | | | 3.50 ± 0.16 | 3.58 |
| 28 | | | | | | | | | 3.43 ± 0.16 | 3.61 |
| 29 | | | | | | | | | 3.65 ± 0.12 | 3.65 |
| 30 | | | | | | | | | 3.82 ± 0.10 | 3.70 |
| 31 | | | | | | | | | 3.91 ± 0.21 | 3.74 |

in Fig. 3(a) and using 2pF density in Fig. 3(b). From the figures, the neutron radius of ^{29}F is obtained as 3.75 ± 0.14 fm using HO density, while using 2pF density it was found to be 3.78 ± 0.15 fm. The neutron radius of ^{29}F obtained here is in good agreement with Ref. [24]. Equally, both HO density and 2pF density yield similar neutron radii for all isotopes and nuclei studied, therefore it suffices to rely on results with HO density only. Interestingly, the neutron configuration for the ground states $0d_{3/2}$ or $1p_{3/2}$ hardly incur any variation in the calculated neutron radii either. The neutron skin thickness of ^{29}F is evaluated to be 0.85 ± 0.14 fm.

The same procedure is repeated for all fluorine, neon, sodium, magnesium and calcium isotopes. Experimental data for the reaction cross section shift on a carbon target at 240 or 280 MeV/n have been reported by several authors [16,19–22,24,25]. The obtained neutron radii are consistent with the corresponding ones calculated using densities from Hartree-Fock-Bogoliubov calculations with the BSK2 Skyrme force [17] and they are given in Table III. It is worth noting that the stable nuclei for neon, sodium, magnesium, and calcium isotopes are ^{20}Ne , ^{23}Na , ^{24}Mg , and ^{42}Ca , respectively. Consequently, the neutron radius for ^{31}Ne , using the HO wave function with the neutron configuration for the ground state $(0s_{1/2})^2(0p_{3/2})^4(0p_{1/2})^2(0d_{5/2})^6(0d_{3/2})^4(1s_{1/2})^2(1p_{3/2})^1$, is found to be 3.80 ± 0.11 fm, which is consistent with that of Refs. [26,27]. In addition, the neutron radii of calcium isotopes obtained in this work are in good agreement with those obtained in Ref. [28]. Nevertheless, in the case of magnesium isotopes, the strong deformation in $^{32,34}\text{Mg}$ has not been taken into account.

The neutron skin of all isotopes of F, Ne, Na, Mg, and Ca is subsequently determined based on the corresponding neutron radii obtained in this work. In Fig. 4, the skin is plotted against the isospin $I = (N - Z)/A$. It can be seen that the skin has a strong correlation with iso-spin. The relation is a straight line with a slope equal to 3.216 ± 0.11 fm. The straight line relation was also predicted in Ref. [29] for nuclei heavier than Ca but at a rather smaller slope of about 0.9 ± 0.15 fm. The


 FIG. 4. The neutron skin deduced in this work as a function of the isospin $(N - Z)/A$. The solid line represents the fitting as explained in the text.

slope of the skin against the isospin in the mass region from 21 to 51 studied in this work is much larger than that found in the mass region from 40 to 238 [29]. Also, Aumann [30] obtained a nearly straight line relation between the neutron skin and mass number for $124 \leq A \leq 134$ nuclei.

IV. CONCLUSION

We have introduced a method to deduce the neutron radii of neutron-rich nuclei. The method requires measur-

ing the reaction cross sections (or interaction cross sections) of both a neutron-rich nucleus and its stable isotope at the same energy per nucleon on a carbon target. We used the available experimental data to deduce the neutron radii of $^{21-29}\text{F}$, $^{21-32}\text{Ne}$, $^{24-35}\text{Na}$, $^{25-38}\text{Mg}$, and $^{45-51}\text{Ca}$ isotopes.

The behavior of the neutron skin of the studied isotopes (in the mass region $A = 21-51$) as a function of their isospin $T = (N - Z)/A$ was found to feature a linear relation at a slope equal to 3.216 ± 0.11 fm. This is three times larger than that deduced in the mass region $A = 40-238$, which reflects the large skin in unstable nuclei.

-
- [1] F. J. Fattoyev, J. Piekarewicz, and C. J. Horowitz, *Phys. Rev. Lett.* **120**, 172702 (2018).
- [2] X. Roca-Maza, G. Colo, and H. Sagawa, *Phys. Rev. Lett.* **120**, 202501 (2018).
- [3] I. A. M. Abdul-Magead, E. Hamza, and B. Abu-Ibrahim, *J. Phys. G: Nucl. Part. Phys.* **47**, 055103 (2020).
- [4] B. Abu-Ibrahim and Y. Suzuki, *Phys. Rev. C* **61**, 051601(R) (2000); **62**, 034608 (2000).
- [5] R. J. Glauber, in *Lectures on Theoretical Physics*, edited by W. E. Brittin and L. C. Dunham (Interscience, New York, 1959), Vol. 1, p. 315.
- [6] J. S. Al-Khalili and J. A. Tostevin, *Phys. Rev. Lett.* **76**, 3903 (1996); J. S. Al-Khalili, J. A. Tostevin, and I. J. Thompson, *Phys. Rev. C* **54**, 1843 (1996).
- [7] B. Abu-Ibrahim, K. Fujimura, and Y. Suzuki, *Nucl. Phys. A* **657**, 391 (1999).
- [8] R. F. G. Ruiz *et al.*, *Nat. Phys.* **12**, 594 (2016).
- [9] H. Heylen, C. S. Devlin, W. Gins, M. L. Bissell, K. Blaum, B. Cheal, L. Filippin, R. F. Ruiz, M. Godefroid, C. Gorges, J. D. Holt, A. Kanellakopoulos, S. Kaufmann, A. Koszorus, K. Konig, S. Malbrunot-Ettenauer, T. Miyagi, R. Neugart, G. Neyens, W. Nortershauser, R. Sanchez, F. Sommer, L. V. Rodriguez, L. Xie, Z. Y. Xu, X. F. Yang, and D. T. Yordanov, *Phys. Rev. C* **103**, 014318 (2021).
- [10] H. De Vries, C. W. De Jager, and C. De Vries, *At. Data Nucl. Data Tables* **36**, 495 (1987).
- [11] J. D. Patterson and R. J. Peterson, *Nucl. Phys. A* **717**, 235 (2003).
- [12] B. Abu-Ibrahim, W. Horiuchi, A. Kohama, and Y. Suzuki, *Phys. Rev. C* **77**, 034607 (2008).
- [13] S. Kox, A. Gamp, C. Perrin, J. Arvieux, R. Bertholet, J. F. Bruandet, M. Buenerd, R. Cherkaoui, A. J. Cole, Y. El-Masri, N. Longequeue, J. Menet, F. Merchez, and J. B. Viano, *Phys. Rev. C* **35**, 1678 (1987).
- [14] A. Ozawa *et al.*, *Nucl. Phys. A* **693**, 32 (2001).
- [15] M. Takechi, M. Fukuda, M. Mihara, K. Tanaka, T. Chinda, T. Matsumasa, M. Nishimoto, R. Matsumiya, Y. Nakashima, H. Matsubara, K. Matsuta, T. Minamisono, T. Ohtsubo, T. Izumikawa, S. Momota, T. Suzuki, T. Yamaguchi, R. Koyama, W. Shinozaki, M. Takahashi, A. Takizawa, T. Matsuyama, S. Nakajima, K. Kobayashi, M. Hosoi, T. Suda, M. Sasaki, S. Sato, M. Kanazawa, and A. Kitagawa, *Phys. Rev. C* **79**, 061601(R) (2009).
- [16] M. Tanaka *et al.*, *Phys. Rev. Lett.* **124**, 102501 (2020).
- [17] IAEA, <https://www-nds.iaea.org/RIPL-3/>.
- [18] R. F. Carlson, *At. Data Nucl. Data Tables* **63**, 93 (1996).
- [19] A. Homma *et al.*, in *Proceedings of the 14th International Symposium on Nuclei in the Cosmos (NIC2016)* (JPS, Tokyo, 2017), p. 021010.
- [20] M. Takechi *et al.*, *Mod. Phys. Lett. A* **25**, 1878 (2010).
- [21] S. Suzuki *et al.*, *EPJ Web Conf.* **66**, 03084 (2014).
- [22] M. Takechi *et al.*, *EPJ Web Conf.* **66**, 02101 (2014).
- [23] H.O. Meyer, P. Schwandt, R. Abegg, C. A. Miller, K. P. Jackson, S. Yen, G. Gaillard, M. Hugi, R. Helmer, D. Frekers, and A. Saxena, *Phys. Rev. C* **37**, 544 (1988).
- [24] S. Bagchi, R. Kanungo, Y. K. Tanaka, H. Geissel, P. Doornenbal, W. Horiuchi, G. Hagen, T. Suzuki, N. Tsunoda, D. S. Ahn, H. Baba, K. Behr, F. Browne, S. Chen, M. L. Cortes, A. Estrade, N. Fukuda, M. Holl, K. Itahashi, N. Iwasa, G. R. Jansen, W. G. Jiang, S. Kaur, A. O. Macchiavelli, S. Y. Matsumoto, S. Momiyama, I. Murray, T. Nakamura, S. J. Novario, H. J. Ong, T. Otsuka, T. Papenbrock, S. Paschalis, A. Prochazka, C. Scheidenberger, P. Schrock, Y. Shimizu, D. Steppenbeck, H. Sakurai, D. Suzuki, H. Suzuki, M. Takechi, H. Takeda, S. Takeuchi, R. Taniuchi, K. Wimmer, and K. Yoshida, *Phys. Rev. Lett.* **124**, 222504 (2020).
- [25] M. Takechi *et al.*, *Phys. Lett. B* **707**, 357 (2012).
- [26] S. Ahmad, D. Chauhan, A. A. Usmani, and Z. A. Khan, *Eur. Phys. J. A* **52**, 128 (2016).
- [27] W. Horiuchi, Y. Suzuki, P. Capel, and D. Baye, *Phys. Rev. C* **81**, 024606 (2010).
- [28] S. Tagami, M. Tanaka, M. Takechi, M. Fukuda, and M. Yahiro, *Phys. Rev. C* **101**, 014620 (2020).
- [29] M. Centelles, X. Roca-Maza, X. Vinas, and M. Warda, *Phys. Rev. Lett.* **102**, 122502 (2009).
- [30] T. Aumann, C. A. Bertulani, F. Schindler, and S. Typel, *Phys. Rev. Lett.* **119**, 262501 (2017).